PERGAMON

International Journal of Solids and Structures 40 (2003) 4989–5000

INTERNATIONAL JOURNAL OF SOLIDS and STRUCTURES

www.elsevier.com/locate/ijsolstr

Numerical investigation of powder compaction of gear wheels

J. Cedergren [a,*], N.J. Sørensen [a], S. Melin [b]

[a] *Division of Mechanics, Lund University, Box 118, SE-221 00 Lund, Sweden*
[b] *Division of Solid Mechanics, Lund University, Box 118, SE-221 00 Lund, Sweden*

Received 30 August 2002; received in revised form 11 December 2002

Abstract

A method to judge the porosity distribution within complex powder compacted 3D structures using a dynamic 3D dilatant finite strain finite element program is presented. The method is demonstrated for a gear wheel, using a combined FKM Gurson model with parameters calibrated from experiments to model a ferrous powder. Compaction is pursued until a final average porosity of 3% in the gear. The method is shown successful in judging the influence on local as well as average properties from change in geometrical parameters and compaction speed.

Keywords: Powder compaction; Friction; Porous material; Gear wheel; Finite elements; Dynamics

1. Introduction

Manufacturing of small precision components through metal powder compaction is becoming an increasingly important industrial technique, offering the possibility of near net shape production of complex geometries with substantial reductions in cost at large scale production as compared to traditional manufacturing. The development of more advanced metal powder compositions together with more refined manufacturing procedures continually open new areas of application. With this development follows increasing demands for methods of controlling the component properties.

One characteristic feature of powder-manufactured (P/M) components is the porosity, governing the mechanical properties of the component. Generally a low porosity, of the order down to a few percent, is preferred. The porosity distribution is, however, not trivial and cannot easily be foreseen. It is not homogenous through the body but dependent on friction between the powder and the die wall during the compaction phase, shape of the body, dynamic effects, and applied pressure.

To determine the porosity distribution within a component through experiments is costly as well as time consuming. In this context, numerical simulation of the compaction process becomes increasingly important, offering possibilities of faster and cheaper component development. However, critical to the success of

* Corresponding author. Tel.: +46-46-222-3039; fax: +46-46-222-4620.
E-mail address: joakim.cedergren@mek.lth.se (J. Cedergren).

0020-7683/$ - see front matter © 2003 Elsevier Ltd. All rights reserved.
doi:10.1016/S0020-7683(03)00250-6

such simulations are proper calibrations of the material models and the capability to capture the influence from three-dimensional features of the component.

A number of attempts to model powder compaction has been undertaken. In Cocks (2001) the current status of models for powder compaction is reviewed, and recent experimental and theoretical studies presented. Redanz (1999) performed a quasi-static 2D axi-symmetric study of powder compaction of a cup shaped geometry, using a rate-independent elastic plastic combined FKM Gurson model (cf. Fleck et al., 1992; Gurson, 1977). Coulomb friction with an upper limit for the friction stress was used to model the contact between the powder and the die. The simulations showed good agreement with experiments for which the final average porosity was about 20%. Wikman (1999) modelled compaction of a 2D L-shaped geometry employing a cap plasticity model (cf. Häggblad, 1991). Coulomb type of friction was used to model the friction between powder and die, and the experiment was used to calibrate the constitutive model. In Kim et al. (1996) a combination of two elastic–plastic constitutive models, the Shima Oyane model (cf. Shima and Oyane, 1976) and the FKM Gurson model were used to model the powder. The friction between powder and die was Coulomb friction with constant coefficient of friction. Input data to the model were taken from experiments with stainless steel powder and tool steel powder, but no validating experiments were performed.

In Cedergren et al. (2002), 3D simulations of compaction of ferrous powder components with circular and rectangular cross-section were conducted. Two constitutive models were compared; the Shima Oyane model and the FKM Gurson model. A modified Coulomb friction law, with the coefficient of friction depending on the compaction pressure, modelled the contact between the die and the powder. The simulations were conducted using a dynamic 3D dilatant finite strain finite element program. Compaction was pursued until a final average porosity of 3%. Experiments with ferrous powder were conducted in order to calibrate the constitutive models. The simulations proved successful in predicting final porosity distribution as compared to experimental evaluations. It was shown that both constitutive models could be used to obtain a reasonable agreement with experiments, indicating that friction had a dominating influence on the outcome of the simulations.

In the present paper compaction of a gearwheel is studied, employing the method described in Cedergren et al. (2002). The influence on the final average porosity distribution from variation in rack parameters, change of number of gear teeth, change of height of the gear, together with influence from compaction speed, is investigated. The goal is to demonstrate the usefulness of the present method for judging local as well as average properties for a complex 3D geometry, such as a standard gear.

2. Problem formulation

A numerical study of double action powder compaction of a gearwheel is conducted. Fig. 1 shows a meshed gear wheel geometry with 20 gear teeth. Only half of a gear tooth is studied due to symmetry. The initial average porosity of the gearwheel is 30.0%, homogeneously distributed, and the gearwheel is compacted to an average porosity of 3.0% at the final stage. Double action compaction is used, i.e. the punch is applied from the top and from the bottom, and the gear tooth is in contact with the die along the inner ring and along the tooth flank. The displacement $U(t)$ of the punch is ramped up to linear time dependency according to

$$U(t) = \begin{cases} -vt^*/\pi(1-\cos(\pi t/t^*)) & 0 \leqslant t \leqslant 0.5t^* \\ -vt^*/\pi(1+\pi t/t^* - \pi/2) & 0.5t^* < t \end{cases} \tag{1}$$

where v is the final punch velocity, t^* is a constant, and t denotes time.

The basic rack measures, following the Swedish standard SMS 296, are shown in Fig. 2, where r_{0t} denotes the fillet radius, α_t the pressure angle, h_{0t} the dedendum, b the factor determining the thickness of the

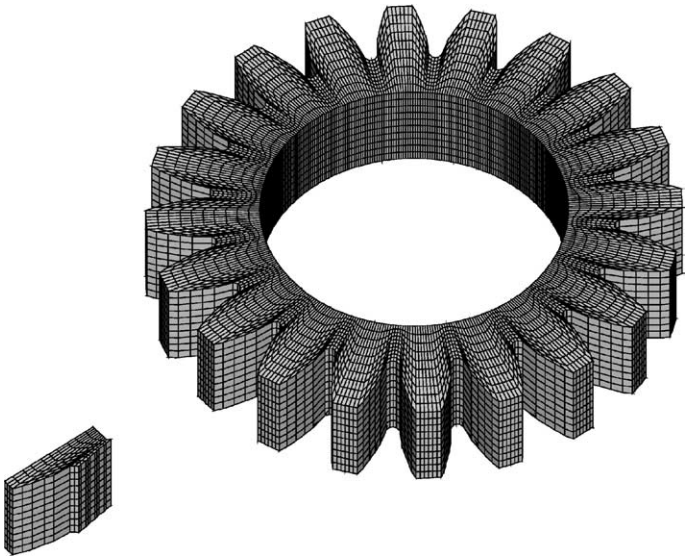

Fig. 1. A gearwheel consisting of 20 gear teeth. One half gear tooth is used in the calculations.

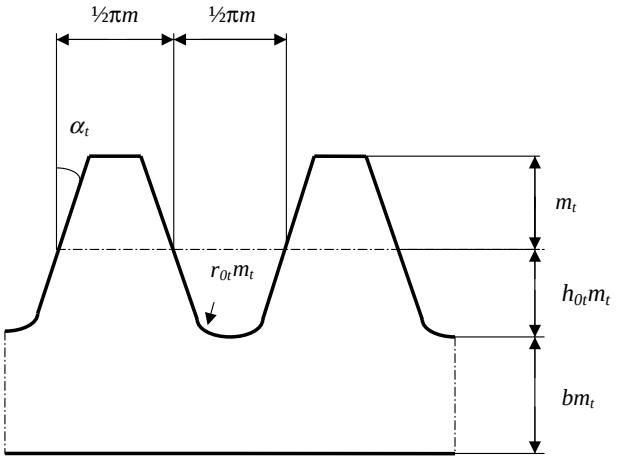

Fig. 2. Basic rack measures following the Swedish standard SMS 292. The fillet radius is denoted r_{0t}, the pressure angel α_t, the dedendum h_{0t}, the factor determining the thickness of the inner ring b, and the basic rack modulus m_t.

inner ring, and m_t the basic rack modulus (cf. Vedmar, 1994). The influence on final porosity distribution from variations of the basic rack parameters according to Table 1, together with the influence from number of gear teeth, z, gear height h, and punch speed, will be investigated.

In this study the combined FKM Gurson model is employed (cf. Fleck et al., 1992; Gurson, 1977; Redanz, 1999). The combined flow potential, Φ_{comb}, is given by

$$\Phi_{\text{comb}} = W_{\text{FKM}}\Phi_{\text{FKM}} + W_{\text{G}}\Phi_{\text{G}} = 0 \tag{2}$$

where W_{G} and W_{FKM} are weight functions and FKM referrers to the FKM model and G to the Gurson model.

Table 1
Parameter combinations investigated

Case	r_{0t}	α_t	h_{0t}	b	m_t (m)	h (m)	z
1	0.38	20°	1.25	2	0.008	0.03	20
2	0.30	20°	1.25	2	0.008	0.03	20
3	0.38	25°	1.25	2	0.008	0.03	20
4	0.38	20°	1.0	2	0.008	0.03	20
5	0.38	20°	1.25	3	0.008	0.03	20
6	0.38	20°	1.25	2	0.004	0.03	20
7	0.38	20°	1.25	2	0.008	0.06	20
8	0.38	20°	1.25	2	0.008	0.03	15

The FKM porous material model by Fleck, Kuhn and McMeeking assumes that spherical particles form the porous material, and is valid at higher porosities only. The particles are joined by isolated contacts. The highest possible porosity f for this model is $f = 0.36$. The flow function is given by

$$\Phi_{\mathrm{FKM}} = \left(\frac{5}{18}\frac{\sigma_e}{p_y} + \frac{2}{3}\right)^2 + \left(\frac{\sqrt{5}}{3}\frac{\frac{1}{3}\sigma_k^k}{p_y}\right)^2 - 1 = 0 \tag{3}$$

where σ_e is the von Mises stress, p_y the yield strength of the porous material under hydrostatic loading, and $\sigma_k^k/3$ the hydrostatic stress.

The Gurson model is based on the assumption that the porous material consists of a matrix containing separated, spherical voids, which is an assumption of the material behavior at the end of the compaction. The potential function for the Gurson model is of the form (cf. Tvergaard, 1990)

$$\Phi_G = \left(\frac{\sigma_e}{\sigma_f}\right)^2 + 2q_1 f \cosh\left(\frac{q_2\sigma_k^k}{2\sigma_f}\right) - q_1^2 f^2 - 1 = 0 \tag{4}$$

where q_1 and q_2 are adjustment factors and σ_f is the yield stress of the matrix material.

The Gurson model is known to perform the best for low porosities and the FKM model is more suited for high porosities. Therefore, a combination of the models can be used to cover the whole event of powder compaction.

The contact between the powder and the die was modelled using Coulomb friction with zero adhesion. A model for the friction coefficient $\mu(T_n)$ is introduced where the friction coefficient decreases as the compressive traction in the normal direction, T_n, increases, and is given by

$$\mu(T_n) = \mu_1 + \mu_2 e^{T_n/T_{n1}} \tag{5}$$

where μ_1, μ_2 and T_{n1} are constants, determined from experiments (cf. Cedergren et al., 2002).

The simulations were performed using a dynamic 3D dilatant finite strain finite element program. In order to make the program as general as possible, viscoplastic effects (cf. Rice, 1970, 1971; Becker and Needleman, 1986) and adiabatic heat generation due to plastic dissipation, (cf. Povirk et al., 1990; Knoche and Needleman, 1993) were added. Twenty node iso-parametric 3D brick elements with 27 integration points per element were used and the contact and friction was modelled by a penalty approach.

The mesh dependence of three dimensional compaction simulations was investigated in Cedergren et al. (2002). Calculations were performed for five different mesh refinements, with the finest mesh consisting of $10 \times 10 \times 20$ elements. The results showed good agreement of the average behavior in different parts of the bricks studied. Maximum and minimum final porosities were of the same order and obtained at the same locations in all cases. It was thus concluded that the overall porosity distribution showed moderate mesh

dependence in the cases of cylindrical and quadratic cross-sections. From these investigations it is expected that the mesh refinement in the present study is sufficient.

3. Simulations and results

The influence from different combinations of geometry parameters according to Table 1 on the final porosity distribution in the gear has been investigated. Case 1 of Table 1 was chosen as the default case, to which all other simulations were compared. For all simulations the same material parameters as in Cedergren et al. (2002) were used to model a ferrous powder. The parameters in Eq. (5) were chosen to $\mu_1 = 0.06$, $\mu_2 = 0.08$, and $T_{n1} = 100$ MPa. The gear was compacted through double action compression in the Z-direction with the velocity v of Eq. (1) equal to $v = 10$ m/s. Rapid ramping was obtained by choosing the parameter t^* of Eq. (1) to $t^* = 0.0001$ s. In addition to the simulations specified by Table 1, for Case 1 one simulation with $v = 25$ m/s and $t^* = 0.0001$ s was performed. Furthermore, a simulation with an artificial gear tooth shape with sinusoidal gear flank has been conducted to investigate the necessity of a correct geometry description. Compaction was perused until a final average porosity of 3.0% in the gear. Due to symmetry the calculations were performed for half a gear tooth, only.

The result from the powder compaction process for Case 1 (default case) is shown in Fig. 3. The contour plot uses nodal values of the field quantities, extrapolated from the element integration points to the nodal points. The extrapolated values associated with all elements connected to a node are averaged. Two different views of half the gear tooth are shown in Fig. 3, one from the gear flank (Fig. 3a) and one from the inner ring (Fig. 3b).

The porosity distribution in Fig. 3 applies to the final stage of compaction, when the average porosity in the gear is 3.0%. The variation in porosity is primarily an effect of friction. If the friction coefficients μ_1 and μ_2 are set equal to zero, only small variations in final porosity are found for the geometries studied in this paper. At early stages of the compaction process, the porosity is evenly distributed in the XY-plane for each Z, with the dominating porosity variations in the Z-direction. As the compaction process progresses, porosity variations spread from the boundary towards the center of the tooth, resulting in a porosity variation also in the XY-plane.

As seen from Fig. 3, the gear becomes more compacted at the top and at the bottom than along the center plane. At the end of the process the largest porosity variations are found along the sides where the

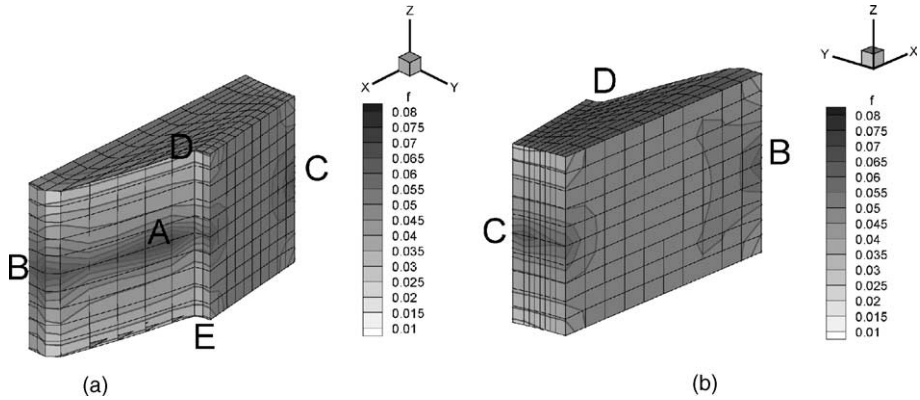

Fig. 3. Contour plot of the final porosity distribution in half a gear tooth for Case 1 in Table 1, to the left a view from the gear flank and to the right from the inner ring.

gear has been in contact with the die. Two local maximum in porosity are found on the gear flank, both along the center plane. One is located close to the gear root, marked A in Fig. 3, where the porosity reaches 6.4%, and one at the top of the gear tooth, B in Fig. 3, with a porosity of 6.0%. In addition, a local maximum occurs along the inner ring at the center plane where the porosity is 5.4%, marked C in Fig. 3. Minimum porosity is found at the gear flank, close to the top and the bottom surfaces (D and E in Fig. 3) where the final porosity reaches 1.3%, only. Since double action compaction is simulated the porosities at D and E are equal due to symmetry. Therefore, only D is referred to below. The porosity distribution within in the gear is more homogenous and varies between 2.5% and 3.0%. The porosity distribution through the gear tooth can be seen from Fig. 4, which is an exploded view of Fig. 3a. Fig. 4 clearly shows the concentration of porosity gradients close to the areas in contact with the die.

Whereas the general trend in porosity distribution within the gear remained between the different geometrical parameter setups specified by Table 1, with local maximum and minimum porosity occurring at approximately the same positions, the extreme value as well as the porosity gradients showed to be more sensitive to geometrical features.

The influence on the final porosity distribution from a lower value of fillet radius, Case 2 in Table 1 with $r_{0t} = 0.30$, is depicted in Fig. 5. The porosity distribution along the gear root showed an increase in porosity distribution gradients as compared to Case 1. The local maximum of porosity at A increased to 6.5%, whereas no significant change in magnitude of maximum porosity was found at positions B and C, or of the minimum porosity at D.

Fig. 6 shows the porosity distribution for Case 3, where the pressure angel α_t has been increased from 20° to 25°, as compared to Case 1. The magnitude of the local maximum porosity at position A decreased to

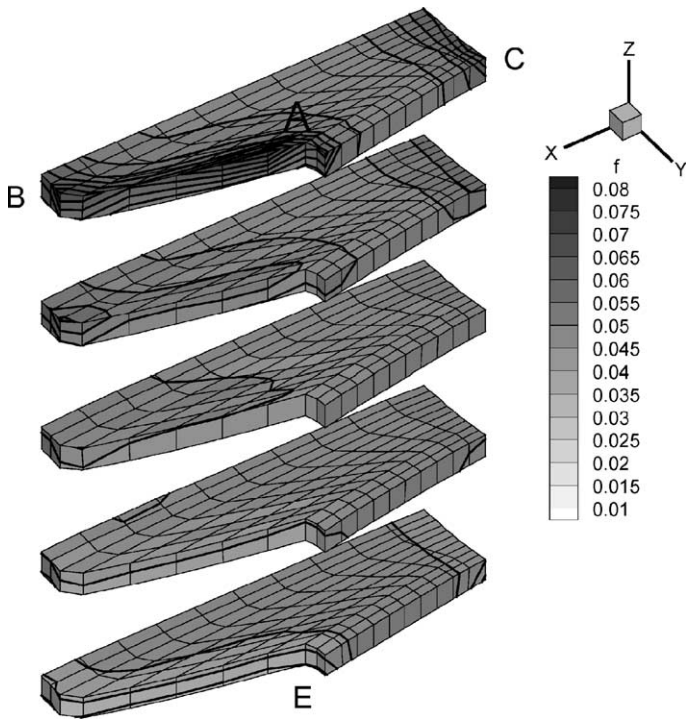

Fig. 4. Exploded plot of lower half of Fig. 3b.

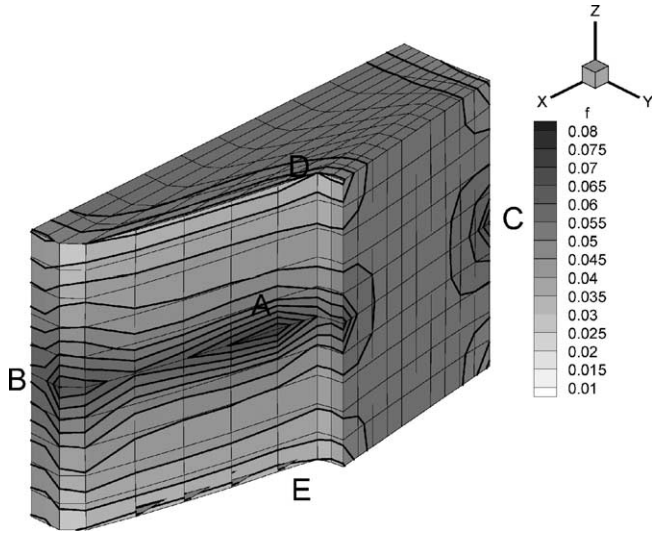

Fig. 5. Contour plot of the final porosity distribution for Case 2.

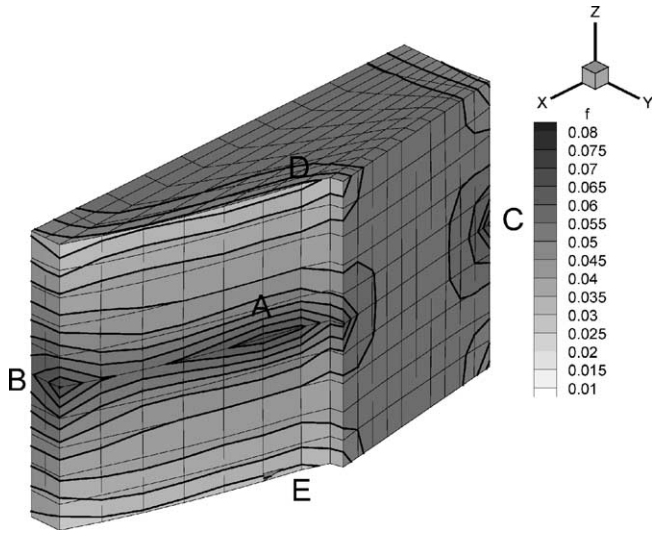

Fig. 6. Contour plot of the final porosity distribution for Case 3.

5.9% whereas no change was observed at position B. The local maximum porosity at C decreased slightly to 5.3%, as did the local minimum value at D, where local minimum porosity of 1.1% resulted.

In Fig. 7 the effect from choosing a shorter gear tooth, Case 4 with h_{0t} reduced from 1.25 to 1.0, is displayed. The shortening of the gear tooth increased the local maximum porosity magnitudes at A to 6.6% and at B to 6.1%. The maximum at C and the minimum at D were unchanged as compared to the default case.

Fig. 8 shows the effects of an increase of the thickness of the inner ring, Case 5 with the factor $b = 3$. The increased thickness of the inner ring reduced the porosity maximum at position A to 5.3%, and at C to

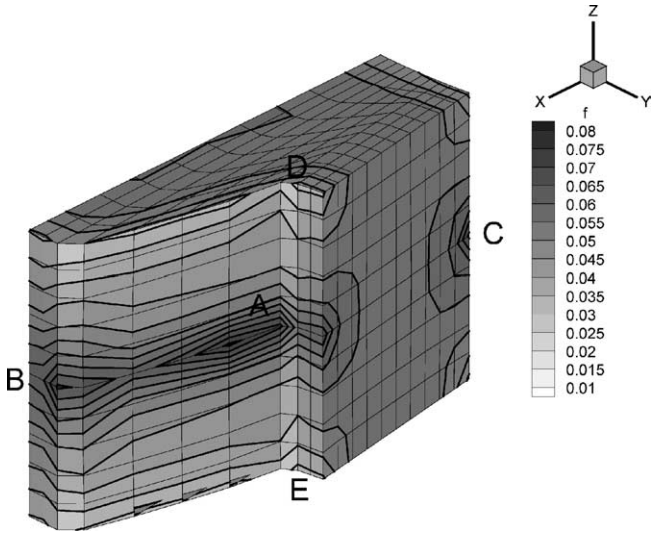

Fig. 7. Contour plot of the final porosity distribution for Case 4.

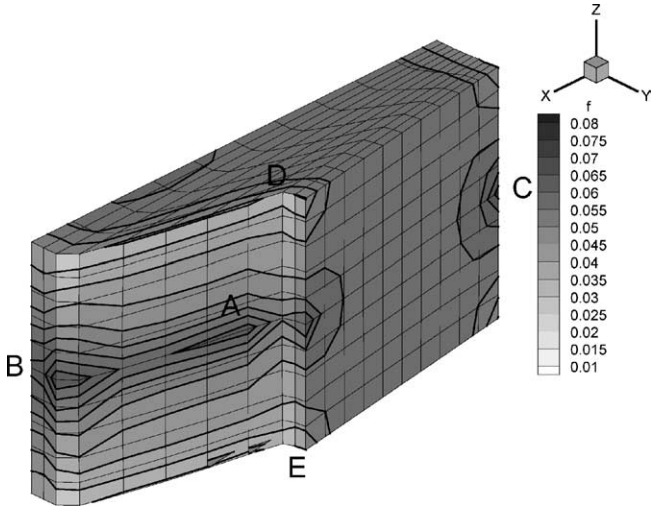

Fig. 8. Contour plot of the final porosity distribution for Case 5.

4.9%, whereas the local maximum at B and the local minimum at D remained unchanged as compared to the default case.

Fig. 9 shows the result for Case 6, where m_t has been reduced to half, resulting in a gear tooth of half the size of the one in Case 1. The local maximum porosity at A decreased to 6.0%. At position B the maximum increased to 7.2% and at position C to 5.9%. The local minimum at D was dramatically reduced to 0.3%, only.

The validity of the simulations was established from comparison of the results between simulations of Case 6 and Case 7. Doubling both the basic rack measure m_t and the gear height h resulted in the same final porosity distribution for both cases.

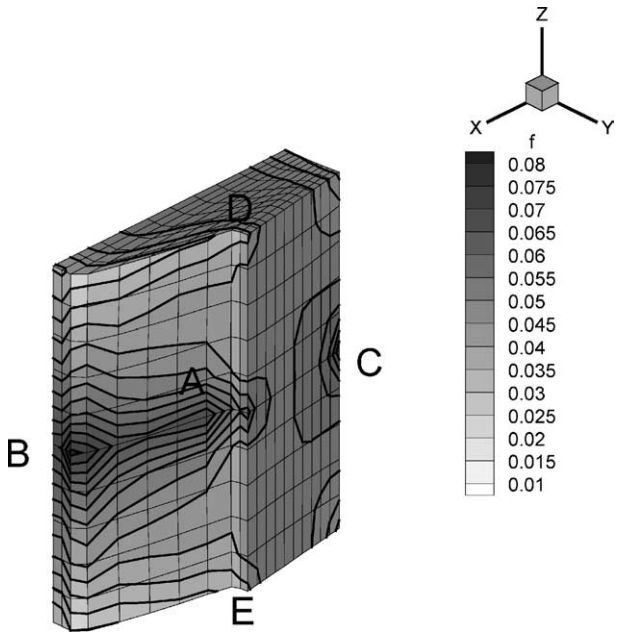

Fig. 9. Contour plot of the final porosity distribution for Case 6.

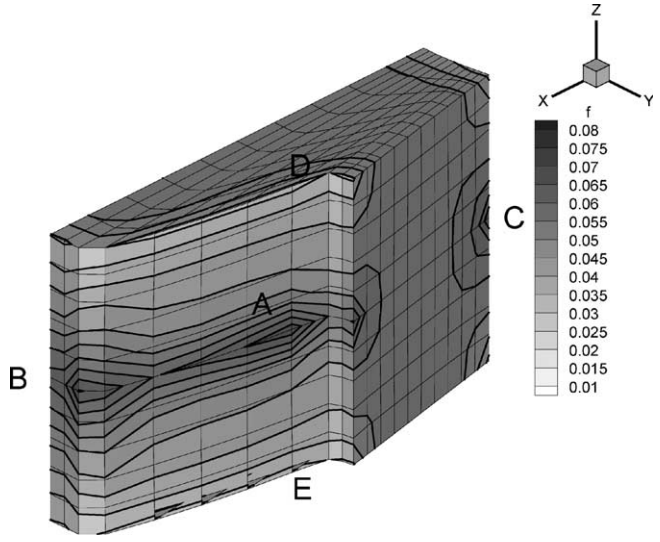

Fig. 10. Contour plot of the final porosity distribution for Case 8.

A decrease in number of gear teeth from 20 to 15 results in a porosity distribution according to Fig. 10. A decrease in local maximum porosity at position A, down to 5.8% resulted, whereas no change in porosity at the local maximum at B and minimum at D where found. The local maximum porosity at C decreased to 5.1%.

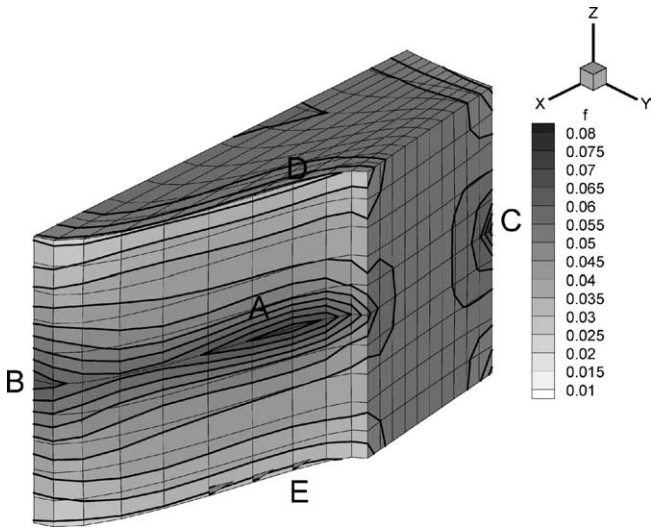

Fig. 11. Contour plot of the final porosity distribution assuming a sinusoidal tooth flank shape.

To investigate the importance of a precise geometry description on the porosity predictions, calculations were conducted with an artificial tooth with sinusoidal tooth flank shape (cf. Fig. 11). The simulation shows no general change in porosity distribution in the local extremes at C and D. The local maximum at A and B decreased however, to 6.3% at A and to 5.7% at B. Thus the relative difference between A and B increased as compared to Case 1. The result suggests that a correct geometry description is a prerequisite for a correct porosity distribution prediction.

The effect of an increase in compaction speed is visualized in Fig. 12, which shows the result after applying a compaction velocity of 25 m/s to the geometry of Case 1. The result is a more homogenous porosity

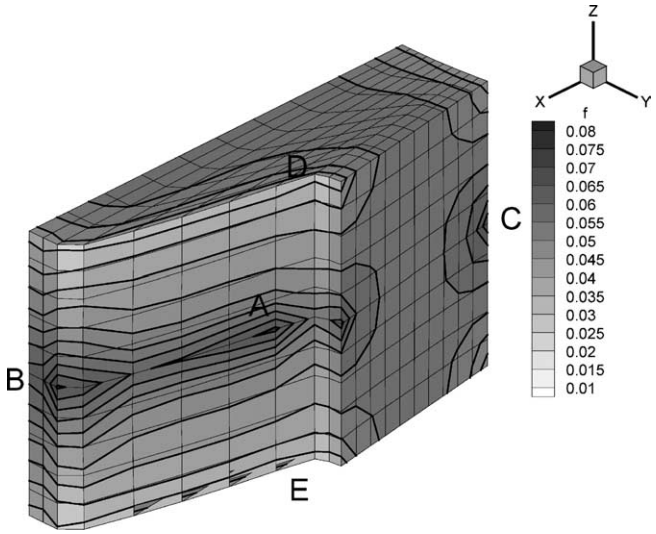

Fig. 12. Contour plot of the final porosity distribution in half a gear tooth for Case 1 assuming a compaction speed of 25 m/s.

distribution. The positions of local maximum and minimum are retained but the maximum porosities have decreased to 5.6% at A, and to 5.0% at C. The maximum at B has increased slightly, to 6.1%. The minimum porosity at D has been reduced to 1.1%.

4. Concluding remarks

The present 3D-analysis of compaction of gears shows, that the porosity distribution in powder compacted gears is somewhat sensitive to various parameters describing the gear geometry. In particular, the number of gear teeth, the thickness of the inner ring and the pressure angle showed to influence the extreme values of the porosity. In most cases, the general trend of the porosity distribution, with maximum and minimum remaining at the same positions within the gear, resulted irrespective of small changes in geometrical parameters. The present dynamic simulations also indicated that an increase in the compaction speed could result in a more homogeneous porosity distribution.

When considering a gear it is of course important that the gear is strongest where it is subjected to the highest load. Two modes of failure are well established for gears, tooth root bending fatigue and contact fatigue. The porosity weakens the material which makes it important to be able to choose rack parameters in combinations that result in an as evenly compacted gear as possible. The present method provides such a tool.

Earlier studies of gears (cf. e.g. Vedmar, 1994) indicate that cyclic loading of gears may give rise to high stress triaxiality that could be dealt with within the present dilatant material model, since the model used is capable of showing damage evolution for cases with hydrostatic tension. Otherwise, the presence of shear strain in realistic loading situations indicates the need for a dilatant material failure model extended with rounded vertex on the instantaneous yield surface to better accumulate a localized failure mode (cf. Mear and Hutchinsson, 1985). In summary, the rather complex geometry of a realistic gear gives rise to porosity distributions during the powder compaction process that are non-trivial to foresee. In that regard the present 3D model seems to provide a simplified overview.

References

Becker, R., Needleman, A., 1986. Effect of yield surface curvature on necking and failure in porous plastic solids. J. Appl. Mech. 108, 491–498.

Cedergren, J., Sørensen, N.J., Bergmark, A., 2002. Three-dimensional analysis of compaction of metal powder. Mech. Mater. 34/1, 43–59.

Cocks, A.C.F., 2001. Constitutive modeling of powder compaction and sintering. Progr. Mater. Sci. 46, 201–229.

Fleck, N.A., Kuhn, L.T., McMeeking, R.M., 1992. Yielding of metal powder bonded by isolated contacts. J. Mech. Phys. Solids 40, 1139–1162.

Gurson, A.L., 1977. Continuum theory of ductile rupture by void nucleation and growth: Part 1. Yield criteria and flow rules for porous ductile media. J. Eng. Mater. Technol. 99, 2–15.

Häggblad, H.-Å., 1991. Constitutive models for powder materials. Powder Technol. 67, 127–136.

Kim, K.T., Lee, H.T., Kim, J.S., Kwon, Y.S., 1996. Analysis for die compaction of metal powders. Mechanics of granular and porous material. In: Fleck, N.A., Cocks, A.C.F. (Eds.), IUTAM Symposium, Cambridge, UK. Kluwer Academic Publishers, Netherlands, Preprint.

Knoche, P., Needleman, A., 1993. The effect of size on the ductility of dynamically loaded tensile bar. Eur. J. Mech. A/Solids 12 (4), 585–601.

Mear, M.E., Hutchinsson, J.W., 1985. Influence of yield surface curvature of flow localization in dilatant plasticity, Report MECH-62. Harvard University, Division of Applied Sciences.

Povirk, G.L., Needleman, A., Nutt, S.R., 1990. An analysis of residual stress formation in Whisker-reinforced Al–SiC composites. Mater. Sci. Eng. A 125, 129–140.

Redanz, P., 1999. Numerical modelling of the powder compaction of a cup. Eur. J. Mech. A/Solids 18, 399–413.

Rice, J.R., 1970. On the structure of stress–strain relations of time-dependent plastic deformations in metals. J. Appl. Mech. (September), 728–738.

Rice, J.R., 1971. Inelastic constitutive relations for solids: an internal-variable theory and its application to metal plasticity. J. Mech. Phys. Solids 19, 433–455.

Shima, S., Oyane, M., 1976. Plasticity theory for porous metals. Int. J. Mech. Sci. 18, 285–291.

Tvergaard, V., 1990. Material failure by void growth to coalescence. Adv. Appl. Mech. 27, 83–151.

Vedmar, L., 1994. On the mass optimization design of external involute spur gears. Transactions of Machine Elements Division, Lund Technical University, Sweden.

Wikman, B., 1999. Modelling and simulation of powder pressing with consideration of friction. Doctoral Thesis, LTU, 1999, p. 33.